THE JOURNAL OF BIOLOGICAL CHEMISTRY VOL. 291, NO. 18, pp. 9425–9437, April 29, 2016


# Carbohydrate-Carbohydrate Interactions Mediated by Sulfate Esters and Calcium Provide the Cell Adhesion Required for the Emergence of Early Metazoans*[S]

Received for publication, December 8, 2015, and in revised form, February 24, 2016 Published, JBC Papers in Press, February 25, 2016, DOI 10.1074/jbc.M115.708958

**Eduardo Vilanova[‡], Gustavo R. C. Santos[‡], Rafael S. Aquino[‡], Juan J. Valle-Delgado[§¶‖1], Dario Anselmetti[**], Xavier Fernàndez-Busquets[§¶‖2], and Paulo A. S. Mourão[‡3]**

*From the [‡]Hospital Universitário Clementino Fraga Filho and Instituto de Bioquímica Médica Leopoldo de Meis, Universidade Federal do Rio de Janeiro (UFRJ), Rio de Janeiro 21941-913, Brazil, [§]Nanomalaria Group, Institute for Bioengineering of Catalonia (IBEC), Barcelona 08028, Spain, [¶]Barcelona Institute for Global Health (ISGlobal), Hospital Clínic-Universitat de Barcelona, Barcelona 08036, Spain, [‖]Nanoscience and Nanotechnology Institute (IN2UB), University of Barcelona, Barcelona 08028, Spain, and [**]Experimental Biophysics and Applied Nanoscience, Faculty of Physics, Bielefeld University, Bielefeld 33615, Germany*

**Early metazoans had to evolve the first cell adhesion mechanism addressed to maintain a distinctive multicellular morphology. As the oldest extant animals, sponges are good candidates for possessing remnants of the molecules responsible for this crucial evolutionary innovation. Cell adhesion in sponges is mediated by the calcium-dependent multivalent self-interactions of sulfated polysaccharides components of extracellular membrane-bound proteoglycans, namely aggregation factors. Here, we used atomic force microscopy to demonstrate that the aggregation factor of the sponge *Desmapsamma anchorata* has a circular supramolecular structure and that it thus belongs to the spongican family. Its sulfated polysaccharide units, which were characterized via nuclear magnetic resonance analysis, consist preponderantly of a central backbone composed of 3-α-Glc1 units partially sulfated at 2- and 4-positions and branches of Pyr(4,6)α-Gal1→3-α-Fuc2($SO_3$)1→3-α-Glc4($SO_3$)1→3-α-Glc→4-linked to the central α-Glc units. Single-molecule force measurements of self-binding forces of this sulfated polysaccharide and their chemically desulfated and carboxyl-reduced derivatives revealed that the sulfate epitopes and extracellular calcium are essential for providing the strength and stability necessary to sustain cell adhesion in sponges. We further discuss these findings within the framework of the role of molecular structures in the early evolution of metazoans.**

Molecular clock estimates, paleobiogeochemical evidence, and the most widely accepted phylogenetic inferences place sponges (phylum Porifera) at the root of the metazoan tree as the oldest extant multicellular animals (1–4). Such ancestry makes modern sponges suitable organisms for studying the cellular and molecular aspects of the evolution of multicellularity (5). A pivotal feature of metazoans is their cell adhesion molecular machinery, which directs the formation and maintenance of a distinctive multicellular morphology (6). In most animals, protein interactions, such as those in the cell junctions of epithelia, mediate cell adhesion (7); however, sponge multicellularity is sustained by a characteristic cell adhesion and recognition mechanism based on specific carbohydrate-carbohydrate interactions (8).

Carbohydrates have vast structural plasticity, ubiquitous distribution in vertebrate and invertebrate tissues, and are commonly associated with the cell surface (9). Carbohydrate self-adhesion is maintained by relatively weak forces that can increase in orders of magnitude upon the multimerization of individual epitopes into polysaccharides (10). Some examples of specific carbohydrate self-interactions include the multivalent binding of Lewis[x] epitopes involved in the first steps of embryogenesis (11), glycolipid-glycolipid interactions controlling cell adhesion, spreading, and motility (12), and self-interactions of sulfated polysaccharides leading to species-specific cell adhesion in sponges (13).

Proteoglycan-like molecules termed aggregation factors (AFs)[4] mediate intercellular adhesion and recognition in sponges (14). The structures of AFs resemble those of aggrecans: large, extracellular membrane-bound, aggregating, and modular proteoglycans (15). In the marine sponge *Microciona*

* This work was supported by grants from Fundação de Amparo à Pesquisa do Estado do Rio de Janeiro (FAPERJ), Brazil; Conselho Nacional de Desenvolvimento Científico e Tecnológico (CNPq), Brazil; Coordenação de Aperfeiçoamento do Pessoal de Nivel Superior (CAPES), Brazil; Fundación Carolina, Spain; BIO2011-25039 and BIO2014-52872-R from the Ministerio de Economía y Competitividad, including FEDER funds, Spain and 2014-SGR-938 from the Generalitat de Catalunya, Spain. The authors declare that they have no conflicts of interest with the contents of this article.

[S] This article contains supplemental Tables S1–S6.

[1] Present address: Dept. of Forest Products Technology, School of Chemical Technology, Aalto University, Aalto 00076, Finland.

[2] To whom correspondence may be addressed: Barcelona Centre for International Health Research (ISGlobal), Centre Esther Koplowitz, planta 1, Rosselló 149-153, Barcelona 08036, Spain. Tel.: 34-93-227-5400 (ext. 4581); Fax: 34-93-312-9410; E-mail: xfernandez_busquets@ub.edu.

[3] To whom correspondence may be addressed: Hospital Universitário Clementino Fraga Filho, Rua Professor Paulo Rocco 255, sala 4a01, Rio de Janeiro 21941-913, Brazil. Tel.: 55-21-39382090; Fax: 55-21-39382090; E-mail: pmourao@hucff.ufrj.br.

[4] The abbreviations used are: AF, sponge aggregation factor; AFM, atomic force microscopy; CMFBSW, calcium and magnesium free artificial sea water; CMFTSW, calcium- and magnesium-free Tris artificial sea water; COSY, correlation spectroscopy; DAF, aggregation factor from *D. anchorata*; DaSP, sulfated polysaccharide from *D. anchorata*; DFS, dynamic force spectroscopy; SMFSF, single molecule force spectroscopy; $F_{max}$, SMFS average dissociation forces; g200, sulfated polysaccharide from *M. prolifera*; HMBC, heteronuclear multiple bound coherence; HSQC, heteronuclear single quantum coherence; MAF, aggregation factor from *M. prolifera*; NOESY, nuclear Overhauser effect correlation spectroscopy; TOCSY, total correlation spectroscopy; pN, piconewtons.

*prolifera* the AF is constructed by a protein core attached to two different carbohydrate units: a small 6-kDa glycan that mediates the interaction of the AF with putative receptors present in the cell membrane and a larger 200-kDa sulfated polysaccharide, which binds homophilically with identical units on the AFs of adjacent cells (13–16).

Certainly, the multivalent self-interactions of sulfated polysaccharides from AFs mediate cell adhesion in sponges (17). Assays using living sponge cells incubated in the presence of antibodies raised against AF glycans or in high concentrations of their homologous sulfated polysaccharides themselves demonstrated that these molecules must be physiologically available to promote cell adhesion (18, 19). Two central features of this self-interaction process are calcium dependence and species specificity, as broadly demonstrated using cell-free techniques, including bead aggregation experiments, affinity chromatography, membrane blot assays, and force spectroscopy (*e.g.* Refs. 13 and 16–20). Studies using single-molecule force spectroscopy have shown that the average self-interaction forces of sulfated polysaccharides from AFs in the presence of calcium lies between 190 and 310 piconewtons, depending on the species studied (13). The binding forces between homologous sulfated polysaccharides from AFs are significantly stronger than between those from different species, confirming the specificity of those interactions (13).

The chemical analysis of AF-sulfated polysaccharides revealed unique structures, with distinct sugar compositions and sulfation patterns for each species studied (*e.g.* Refs. 21–23). Moreover, these sulfated polysaccharides present highly complex compositions, with several different sugars per motif, including acidic sugars such as pyruvated-galactose and hexuronic acid (23). The presence of sulfate and carboxyl groups is an important chemical feature of these molecules because they represent sites for anionic charged ligands (24).

Currently the AF-mediated mechanism of sponge cell adhesion has been thoroughly characterized; however, the chemical nature of the homophilic and calcium-dependent interactions between their sulfated polysaccharides were only speculated (20, 25–27). Therefore, to further investigate the epitopes involved in these interactions, we determined the self-binding capabilities of native and chemically modified (carboxyl-reduced and desulfated) sulfated polysaccharides purified from the marine sponge *Desmapsamma anchorata* (DaSP) using affinity chromatography, bead aggregation assays, and atomic force microscopy (AFM) single molecule force spectroscopy (SMFS) and dynamic force spectroscopy (DFS). The supramolecular structure and self-binding force profile of the AF from *D. anchorata* (DAF) was described using AFM imaging and SMFS, and the complex and unique structure of its sulfated polysaccharide was fully determined using solution nuclear magnetic resonance (NMR). Overall, the data obtained further elucidate the self-interaction mechanism in AF-sulfated polysaccharides, which are then discussed within the context of the role of early cell adhesion in the evolution of metazoans.

## Experimental Procedures

*Sponge Samples*—The marine sponge *D. anchorata* was collected at Ilha Grande Bay, Brazil. Sponge samples collected for the extraction of sulfated polysaccharides were immediately fixed in 70% ethanol. Samples collected for the extraction of aggregation factors were transported to the laboratory immersed in seawater and maintained in an aquarium at 18 °C until further utilization.

*Isolation and Purification of Cell Surface Aggregation Factors*—Fresh samples of *D. anchorata* were rinsed in calcium- and magnesium-free artificial sea water (CMFBSW) (0.49 M NaCl, 11 mM KCl, 7 mM $Na_2SO_4$, 2.1 mM $NaHCO_3$ (pH 7.4)), cut into small pieces, incubated in CMFBSW for 4 h at 4 °C, squeezed through a 210-mm nylon mesh, and then centrifuged to remove cells and large particles. Proteoglycans were precipitated by increasing calcium concentration to 30 mM. The gel-like precipitate was homogenized in CMFBSW supplemented with 20 mM Tris (CMFTSW) and 2 mM $CaCl_2$, and proteoglycans were precipitated at 35,000 × *g* for 3 h at 4 °C. Purification of aggregation factor was performed via centrifugation in a cesium chloride gradient (50% CsCl in CMFTSW + 2 mM $CaCl_2$) at 38,000 × *g* for 48 h at 4 °C. Purified aggregation factor was dialyzed against CMFTSW + 2 mM $CaCl_2$ and stored in 0.05 $NaN_3$ for further utilization. Protein concentration was determined using a bicinchoninic acid kit (Sigma).

*Extraction and Purification of Sulfated Polysaccharides*—Samples of *D. anchorata* were cut into small pieces, immersed three times in acetone, and dried at 60 °C. Total sulfated polysaccharides were extracted from the dried tissues (100 g) via extensive papain digestion. The extracts were partially purified via cethylpyridinium and ethanol precipitations, as described for other invertebrate tissues (28). Approximately 500 mg (dry weight) of crude extracts were obtained for each batch. These crude extracts (50 mg) were applied to a DEAE-cellulose column (Sigma) equilibrated with 5 mM sodium acetate (pH 5.0) supplemented with 5 mM EDTA (Sigma) and linked to a HPLC system (Shimadzu). The sulfated polysaccharide was eluted from the column using a linear gradient of 0 to 3 M NaCl at a flow rate of 1 ml·min$^{-1}$. Fractions of 0.5 ml were collected and checked via a metachromatic assay using 1,9-dimethylmethylene blue (28) and by measuring conductivity to estimate NaCl concentration. The fractions containing the sulfated polysaccharide were pooled, dialyzed against distilled water, and lyophilized.

*Agarose Gel Electrophoresis*—Purified DaSP (15 μg) and a mixture of standard glycosaminoglycans (dermatan sulfate, heparan sulfate, and chondroitin 6-sulfate; 5 μg of each; Sigma) were applied to an agarose (0.5%) gel. The electrophoresis was run for 1 h at 110 V in 0.05 M 1,3-diaminopropane acetate (pH 9.0). Sulfated polysaccharides in the gel were fixed with 0.1% *N*-cetyl-*N*,*N*,*N*-trimethylammonium bromide solution for 12 h, dried, and then stained with 0.1% toluidine blue in 0.1:5:5 (v/v) acetic acid:ethanol:water.

*Molecular Weight Determination*—Molecular weight of purified DaSP (1 mg) was determined via gel permeation chromatography using a Superose 12 HR 16/70 column (GE Healthcare) linked to a HPLC system (Shimadzu) equilibrated with 20 mM Tris-HCl, 5 mM EDTA, and 0.5 M NaCl (pH 7.4). Dextrans with different molecular masses (300, 150, 60, and 25 kDa; Sigma) were used as standard molecular weight markers. The polysaccharides were eluted from the column using the equili-

bration buffer at a flow rate of 0.5 ml·min$^{-1}$ and monitored by differential refractive index.

*Chemical Analysis of Native and Modified DaSP*—The chemical analysis was performed as described elsewhere (19). Briefly, total hexose and pyruvated-sugar contents were estimated by the phenol-$H_2SO_4$ reaction and carbazole reaction, respectively. After acid hydrolysis of the polysaccharides (6.0 M trifluoroacetic acid for 5 h at 100 °C), sulfate was measured by the $BaCl_2$-gelatin method. The percentage of different monosaccharides was estimated by gas-liquid chromatography of derivative alditol acetates.

*Analysis of DaSP by Nuclear Magnetic Resonance*—$^1$H and $^{13}$C one-dimensional and two-dimensional NMR spectra of native DaSP were recorded using a Bruker DRX 800 MHz apparatus (Bruker) with a triple resonance probe, as detailed previously (29). About 20 mg of DaSP were dissolved in 0.5 ml of 99.9% deuterium oxide (Cambridge Isotope Laboratory). All spectra were recorded at 50 °C with HOD suppression by presaturation. One-dimensional $^1$H NMR spectrum was recorded with 16 scans. Two-dimensional $^1$H,$^1$H COSY (correlation spectroscopy), NOESY (nuclear Overhauser effect correlation spectroscopy), TOCSY (total correlation spectroscopy), $^{13}$C,$^1$H multiplicity-edited HSQC (heteronuclear single quantum coherence), and $^{13}$C,$^1$H HMBC (heteronuclear multiple bound coherence) spectra were recorded using states-time proportion phase incrementation for quadrature detection in the indirect dimension. Phase-sensitive $^1$H,$^1$H TOCSY spectra were run as previously described (30, 31) with 4046 × 400 points with a spin-lock field of 10 kHz and a mix time of 80 ms. $^{13}$C,$^1$H HSQC spectra were run with 1024 × 256 points and globally optimized alternating phase rectangular pulses for decoupling. $^{13}$C,$^1$H HMBC spectrum was recorded with 1024 × 256 points, with a 60-ms delay for evolution of long-range couplings and was set with no decoupling during acquisition time. Chemical shifts are displayed relative to external trimethylsilylpropionic acid at 0 ppm for $^1$H and relative to methanol for $^{13}$C.

*Chemical Modifications of DaSP*—Native DaSP (50 mg) was submitted to desulfation or carboxyl-reduction reactions. Desulfation of DaSP was performed via solvolysis (two rounds) in dimethyl sulfoxide/methanol (9:1, v/v) at 80 °C for 6 h, as previously described (32). Reduction of the carboxyl groups present in pyruvated sugars was carried out using 1-ethyl-3-(3-dimethylaminopropyl)carbodiimide-$NaBH_4$ as previously described (33). Modified DaSP were concentrated using 100-kDa Amicon filtration units (Millipore) and then lyophilized. The effectiveness of these chemical modifications was checked via chemical analysis as described above.

*Affinity Chromatography*—Native DaSP was coupled to Sepharose CL-4B (Sigma) using a standard coupling procedure. Briefly, 50 mg of the native DaSP in 5 ml of coupling solution (50 mM NaCl, 100 mM $NaHCO_3$ (pH 8.2)) were mixed with 3 ml of cyanogen bromide-activated Sepharose CL-4B, and coupling was carried out as described by the manufacturer (Sigma). Affinity chromatographies were carried out using two different solutions: 10 mM phosphate buffer pH 7.0 supplemented with 10 mM $CaCl_2$ or 5 mM EDTA. Native, desulfated, or carboxyl-reduced DaSP (1 mg of each) were applied to the column (3 ml), linked to a HPLC system (Shimadzu), and eluted using a linear gradient of 0 to 3 M NaCl at 0.5 ml·min$^{-1}$. Fractions of 0.5 ml were collected and checked for hexose content (19) and by measuring conductivity to estimate NaCl concentrations.

*Beads Aggregation Assay*—Briefly, 5 × $10^8$ freshly sonified amidine-modified fluorescent latex beads (1 μm in diameter, Life Technologies) were incubated with native, desulfated, or carboxyl-reduced DaSP (2 mg·ml$^{-1}$) in CMFTSW supplemented with 2 mg of EDAC (*N*-(3-dimethylaminopropyl)-*N*′-ethylcarbodiimide; Sigma) and 1 mg of S-NHS (*N*-hydroxysulfosuccinimide; Sigma) overnight at 4 °C and then washed in CMFTSW. The coupling efficiency was determined by measuring the hexose content (19) on the beads after reversing the EDAC/S-NHS cross-linking through acid hydrolysis. Approximately $10^7$ beads coated with native or modified DaSP were diluted in 600 μl of CMFTSW supplemented with 10 mM $CaCl_2$ or 5 mM EDTA and incubated for 1 h with gentle shaking. Images of bead aggregates were acquired using an EVOS FL microscope (Life Technologies). The number of aggregates was calculated using the imaging analysis software Leica QWin (Leica). All of the assays were made in triplicate, and the number of aggregates was compared via analysis of variance using Origin-Pro 8.0 (OriginLab).

*Atomic Force Microscope Imaging*—DAF AFM imaging was acquired under ambient conditions in the tapping mode of operation using standard monolithic Si cantilevers Tap300AI (NanoAndMore) on a commercial instrument Multimode Nanoscope IIIa (Veeco). Substrate muscovite mica surfaces (Plano) were gas phase-silanized with aminopropyl triethoxysilane (Sigma) in a desiccator and overlaid with 50 μl of DAF solution (0.5 mg·ml$^{-1}$) for 15 min at room temperature. Subsequently, the samples were washed with Milli-Q water and dried under $N_2$ flow.

*Single-molecule Force Spectroscopy Assays*—A MFP-3D atomic force microscope (Asylum Research) was used to measure the self-binding forces between DAF and native and chemically modified DaSPs. DAF was adsorbed on gold-coated NPG cantilevers (Bruker), and gold substrates were prepared according to the template-stripped gold method (34). DAF adsorption was performed overlaying the gold-coated cantilevers and substrates with a solution of 0.5 mg·ml$^{-1}$ purified DAF in CMFTSW + 2 mM $CaCl_2$ for 1–2 h at room temperature. Native, carboxyl-reduced, and desulfated DaSP were immobilized on mica substrates and on silicon nitride tips of NP-S cantilevers (Bruker) through a *N*-hydroxysuccinimide-poly-(ethylene glycol)-maleimide (NHS-PEG-MAL) linker of 4750 Da (Iris Biotech GmbH). An amount of 10 μM native, carboxyl-reduced, or desulfated DaSP was incubated with 10 μM NHS-PEG-MAL in deionized water for 2 h at 4 °C. Mica substrates and cantilevers were gas phase-silanized with 3-aminopropyl triethoxysilane (Fluka) in a desiccator and then overlaid with the DaSP-linker solutions at room temperature for 2 h. After incubation, the functionalized substrates and cantilevers were rinsed several times with CMFTSW to remove loosely bound molecules. SMFS experiments were carried out at room temperature by approaching and separating the functionalized cantilevers and substrates in CMFTSW supplemented with 10 mM $CaCl_2$ or 5 mM EDTA. The spring constant of each cantilever was determined using the thermal noise method (35). The same

cantilever and substrate were used for experiments conducted with $CaCl_2$ and EDTA, in the same order. Approximately 2000 force curves were recorded with constant approach velocity (2000 nm·s$^{-1}$) and four different retract velocities (200, 800, 2000, and 5000 nm·s$^{-1}$). The force curves were analyzed with a custom-made MATLAB-based software (Math Works) to calculate the molecular adhesion forces and elasticities. Force histograms were fitted to normal curves to obtain the average dissociation forces ($F_{max}$). For the DFS assays, the loading rates were calculated by multiplying the retracting velocity by the molecular elasticity of each force curve and then analyzed according to the stochastic Bell-Evans model of a forced dissociation under an external load (36).

## Results

*Aggregation Factor of D. anchorata Has a Circular Pattern and Multiple Intermolecular Binding Sites*—Images of DAF acquired via high resolution AFM revealed a proteoglycan remarkably similar to the AF of the sponge *M. prolifera* (MAF) described elsewhere (8, 14, 15), which enabled us to trace parallels between their structures, compositions, and chemical behaviors. DAF has a sunburst-shaped core constructed by a ring, ~130 nm across, and radiating arms up to 190 nm in length (Fig. 1*A*). The ring is composed of ~20 globular units 2 nm high (Fig. 1*A*, *arrowhead 1*), from each of which an arm was protruding. The arms are composed of smaller globular units 1 nm high (Fig. 1*A*, *arrowhead 2*). Shorter and thinner structures attached to the globular proteins of the ring (Fig. 1*A*, *arrow*) represent the sulfated polysaccharides (DaSP) of this aggregation factor.

We evaluated the self-interactions between DAF measuring their self-binding forces in the presence of CMFTSW supplemented with 10 mM $CaCl_2$ using SMFS (Fig. 1*B*). Some of the force curves obtained presented a saw-tooth profile in which each peak represents an intermolecular binding event between one DaSP attached to the tip and another attached to the surface (Fig. 1*C*). The binding efficiency of DAF self-interaction in the presence of calcium was high, with ~78% of approach-retract cycles resulting in adhesion (Fig. 1*D*). The average force ($F_{max}$) measured at a retract velocity of 2000 nm s$^{-1}$ for the last DAF self-adhesion event was 273 ± 6 pN (Fig. 1*D*) and was in the same order of magnitude as MAF self-interaction forces (14). DAF self-interaction forces measured in experiments conducted in lower concentrations of calcium (2 mM) were weaker (data not shown), in agreement with previous SMFS studies using MAF (37). However, this observation requires careful interpretation because the integrity of AF protein cores depends on a residual calcium concentration (14). The data used to calculate the $F_{max}$ were restricted to the last peak of the force curves to ensure that only single molecule self-interaction forces were taken into consideration. The striking supramolecular similarities with MAF clearly place DAF within the family of circular proteoglycans from sponges, the spongicans (15). This finding is consistent with the phylogenetic kinship of *D. anchorata* and *M. prolifera*; both of these species belong to the sponge order Ceractinomorpha (38).

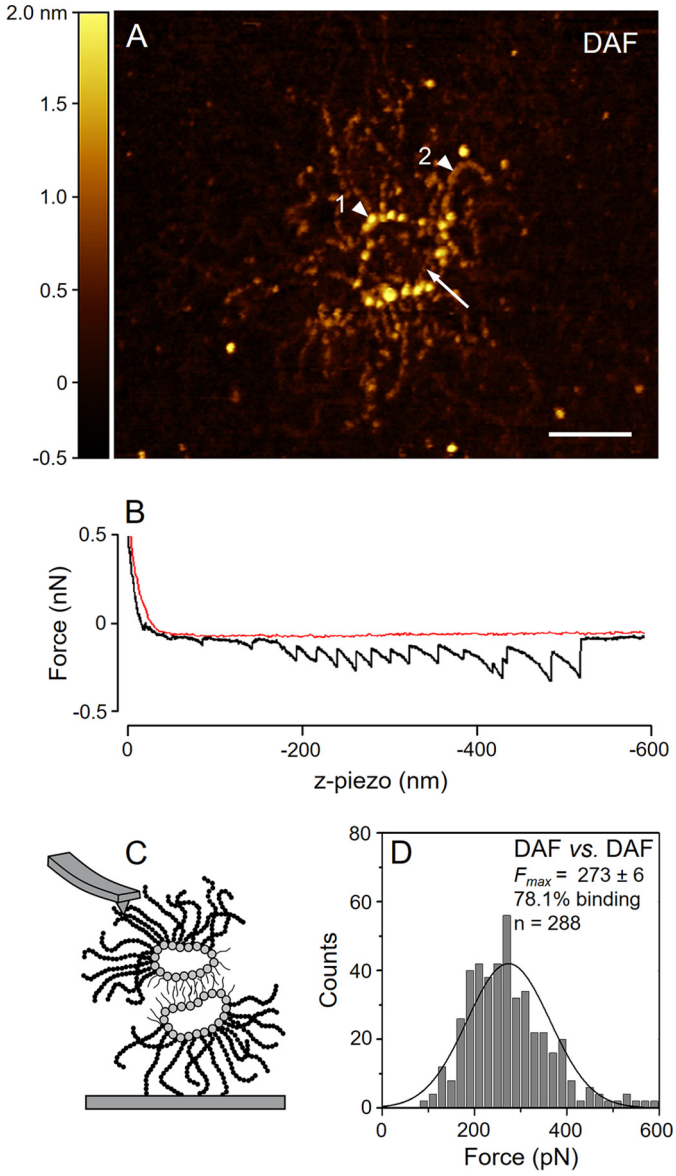


FIGURE 1. **Molecular structure and self-interaction profile of purified DAF.** *A*, high resolution AFM image of DAF. *Arrowheads* indicate the sunburst-shaped protein core composed of a ring (1▶) and several arms (2▶). The *arrow* indicates the position of DAF-sulfated polysaccharides (DaSP). *Scale bar* = 100 nm. *B*, typical saw-tooth profile of a DAF self-interaction. SMFS curve obtained in the approach (*red*) and retract (*black*) cycles. *C*, schematic drawing of the expected topography of interacting DAF molecules in SMFS experiments, modified from Fernàndez-Busquets *et al.* (15). *D*, force histogram of DAF self-interaction forces for the last binding events measured at a retraction velocity of 2000 nm·s$^{-1}$; the *inset* value for $F_{max}$ refers to the mean ± S.E. pN. The self-interaction assays (*panels B* and *D*) were performed in CMFTSW supplemented with 10 mM $CaCl_2$.

*DaSP Is a Highly Branched Sulfated Polysaccharide with a Complex Structure*—DaSP, extracted directly from tissues of the sponge, eluted as a single and sharp peak with ~1.4 M NaCl on anion-exchange chromatography (Fig. 2*A*). Agarose gel electrophoresis confirmed the uniqueness and purity of DaSP; we observed a single and homogeneous band stained with toluidine blue (Fig. 2*B*). Gel permeation chromatography revealed that DaSP has an average molecular mass of ~200 kDa (Fig. 2*C*), which is similar to the sulfated polysaccharide (g200) of MAF (22). Purified DaSP contains glucose, fucose, and galactose at a

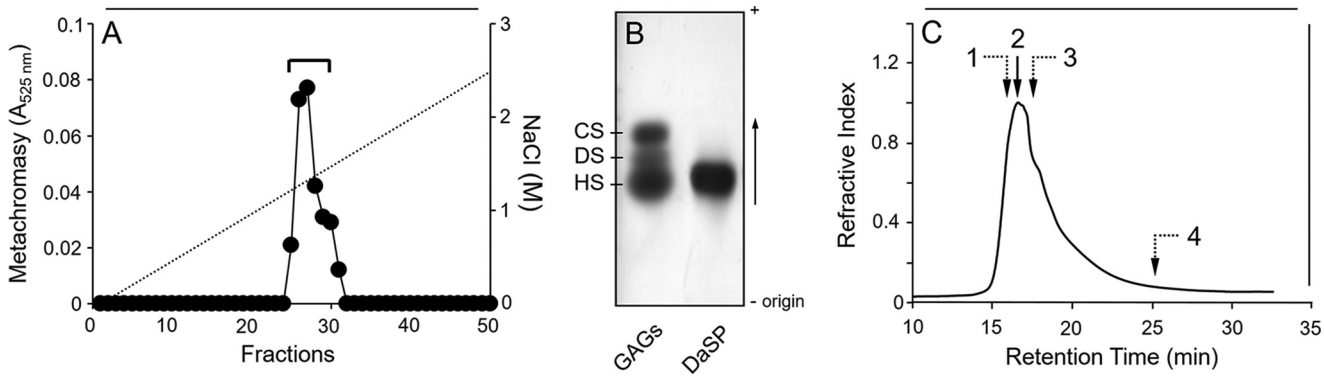


FIGURE 2. **Purification of DaSP.** *A*, DaSP purified (*horizontal bar*) via ion exchange chromatography. *B*, agarose gel electrophoresis of DaSP after purification and a mixture of standard glycosaminoglycans (*GAGs*): heparan sulfate (*HS*), dermatan sulfate (*DS*), and chondroitin sulfate (CS). *C*, molecular weight of DaSP estimated via gel permeation chromatography on Superose 12. *Arrows* indicate the retention time of DaSP (*2*) and dextrans with different $M_r$ values: 300 kDa (*1*); 150 kDa (*3*), and 25 kDa (*4*).

7.5:1.7:0.8 molar ratio as determined via gas chromatography/mass spectroscopy analysis of the derived alditol acetates (data not shown). The molar ratio of the sulfate:total sugar is ~0.66.

The chemical structure of DaSP was investigated using two-dimensional NMR solution analysis. The $^1$H,$^1$H COSY (data not shown), $^1$H,$^1$H TOCSY (Fig. 3, *A* and *B*), and $^{13}$C,$^1$H HSQC (Fig. 4*A*) spectra showed several distinct spin systems, resonating in the region of α-anomers, denoting a polysaccharide with an intricate arrangement of units and a high degree of heterogeneity. A cluster of closely related signals was observed at the 5.20–5.45-ppm region of the spectrum. Two sets of more distinct spin systems were shifted down-field at 5.70 and 5.46 ppm (named D and B units, respectively), whereas another set was up-field at 5.11 ppm (named E unit). The B system was easily assigned to 3-linked, 2,4-disulfated α-glucose units due to the characteristic ~7 ppm down-field of $^{13}$C signal at the glycosylation site and of ~0.6 ppm of the $^1$H signal at the sulfation sites (39, 40). A comparison of chemical shift values for unit B with standard compounds (41–43) can be found in supplemental Table S1. The $^{13}$C chemical shifts of unit B are similar to those observed for a 3-linked and 2,4,6-trisulfated α-glucan (42, 43), except for C6, as expected. The spin system D was also easily identified. The occurrence of a $CH_3$ signal at a very far high-field (1.23/16 ppm) and the anomeric signal at 5.46/96.34 ppm indicate this is an α-fucose residue. Again, as observed for residue B, the marked down-field shift of C3-signal indicates that this is the glycosylation site in unit D. A comparison with standard compounds (40, 44, 45) is provided in supplemental Table S2. Sulfation at position 2 is assured by the 0.6 ppm down-field shift of the H2-signal. The spin system E was assigned to a non-reducing terminal and non-sulfated α-galactose because no significant $^{13}$C or $^1$H shifts (supplemental Table S3) were observed for this residue compared with standard compounds (41, 45, 46).

In addition to these three sets of easily identified signals, we were also able to detect distinct spin systems in the complex region at 5.20–5.45 ppm. These systems belong to 3-linked α-glucose, as indicated by the clear $^{13}$C down-field shift at position 3 (supplemental Table S1). However, they vary on sulfation at position 4, as indicated by the ~0.6 ppm $^1$H down-field shift at position 4. Residue F is 4-sulfated, whereas residues A, C, and G are non-sulfated. Residue C is particularly distinct due to the strong $^{13}$C down-field at positions 3 and 4, indicating that this is a branching point of the polysaccharide, with two glycosylation sites. Residues A and G are both apparently 3-linked, non-sulfated α-glucose units that differ slightly regarding their chemical shifts due to the influence of neighboring residues. A small amount of 6-sulfation may also occur in the sponge polysaccharide, as indicated by the down-shift of $CH_2$ (see anti-phase signal, indicated in *red* in Fig. 4*A*). However, we were not able to identify the unit bearing this sulfation site.

Therefore, the sponge polysaccharide is composed of a complex mixture of residues, including 3-linked α-glucose units that vary in their sulfation sites at the 2- and 4-positions as well as 2-sulfated, 3-linked α-fucose and terminal non-sulfated α-galactose. The next aspect to clarify was the sequence of these residues in the polysaccharide structure. This aspect was initially investigated via a phase-sensitive $^1$H,$^1$H TOCSY spectrum (Fig. 3*B*), which discerns signals of intraresidue spin systems from those of interresidue rotating-frame Overhauser effects (30, 31). This approach allows determination of the saccharide order and linkage position through the correlation of anti-phase (indicated in *red* and their connections by the *horizontal broken lines*) and in-phase (shown in *blue* in the panel and their connections indicated by the *vertical broken lines*) signals (Fig. 3*B*). Briefly, the most intense anti-phase signal shows the linkage in the subsequent sugar residue. The non-reducing terminal α-galactose (residue E) connects with 2-sulfated α-fucose (residue D), which in turn connects with 4-sulfated α-glucose (residue F) and finally with residue G of non-sulfated α-glucose. These four sets of signals constitute the branches of the polysaccharide. The 2,4-disulfated α-glucose (residue B) connects with the major sets of 3-linked α-glucose residues, which constitute the polysaccharide backbone.

The sequence of residues on the sponge polysaccharide was confirmed using $^{13}$C,$^1$H HMBC (Fig. 3*C*). This spectrum enabled us to trace contact between the anomeric $^{13}$C of each unit and $^1$H of the position involved in the glycosidic linkage of the subsequent residue (contact points, H3 and H4 in the case of the sponge polysaccharide, see supplemental Table S4). We identified contact between residues E-D, D-F, F-G, G-C, C-B, A-A, B-A, and A-C, thereby confirming that this is the sequence in the polysaccharide structure. The $^{13}$C chemical shifts of the

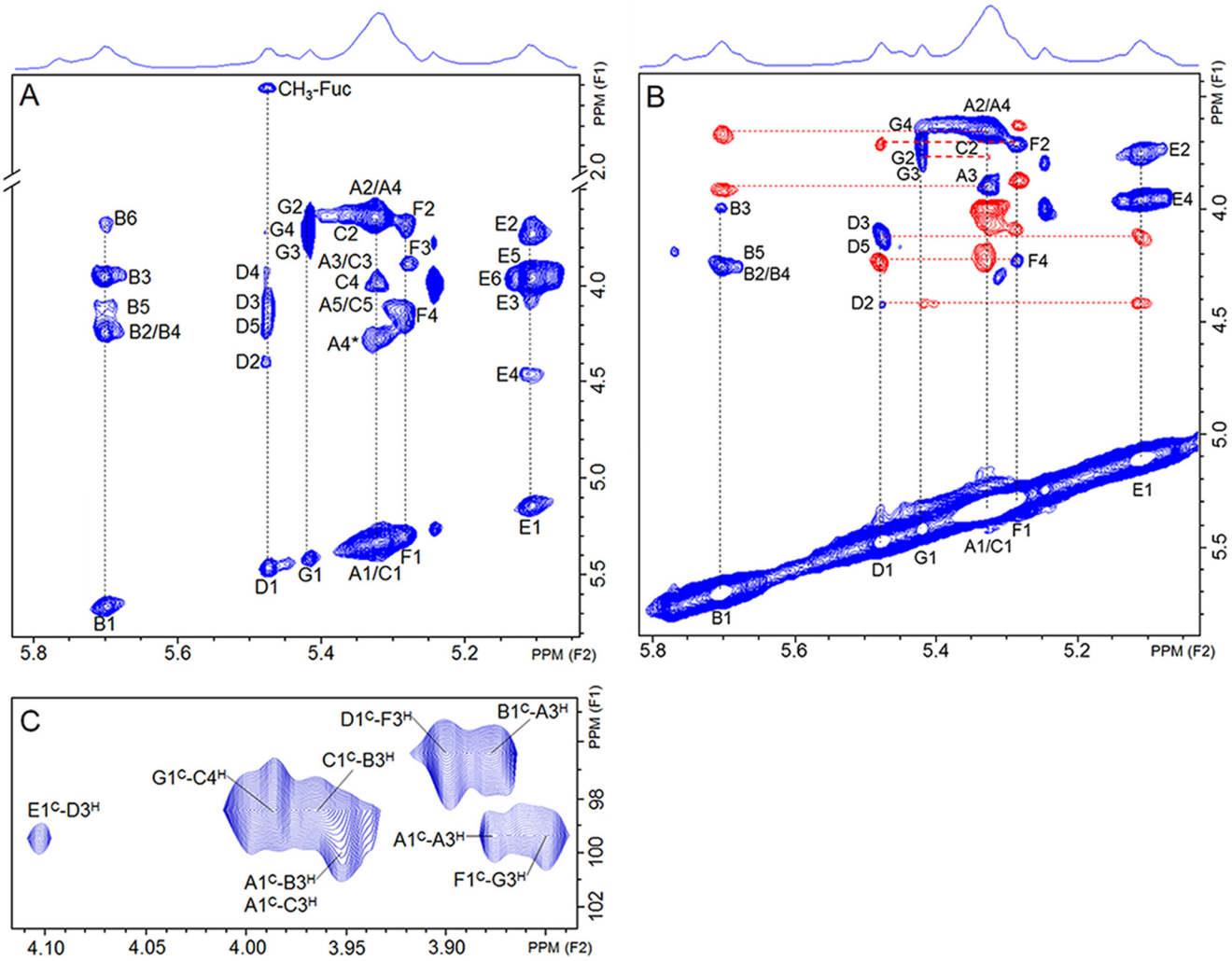


FIGURE 3. **Solution NMR analysis of DaSP.** *A*, $^{1}H,^{1}H$ TOCSY spectrum. *B*, phase-sensitive $^{1}H,^{1}H$ TOCSY spectrum. Signals of the spin systems are on in-phase, indicated in *blue*, whereas signals from the neighboring residues are in anti-phase, indicated in *red*. *C*, $^{13}C,^{1}H$ HMBC spectrum showing the contact points between saccharide units of DaSP.

pairs D1-B1 and G1-C1 (Fig. 3*C*) are close and thus difficult to identify unambiguously. It was clarified analyzing the interresidues rotating-frame Overhauser effects on the phase-sensitive $^{1}H,^{1}H$ TOCSY (Fig. 3*B*). Furthermore, the $^{1}H,^{1}H$ NOESY spectrum (data not shown) presents cross-peaks between: B ($^{1}H1$) and A ($^{1}H3$); G ($^{1}H1$) and C ($^{1}H4$); D ($^{1}H1$) and F ($^{1}H3$). NOE signals connecting residues C and B were not identified due to an intense overlapping of signals on this spectrum.

We were not able to assign some signals on the TOCSY and HSQC spectra due to their low intensity and/or absence of corresponding assignable signals on the HMBC spectrum. Those few unidentified units indicate a certain degree of heterogeneity in DaSP structure, as usually observed in most natural sulfated polysaccharides.

Finally, we also identified the occurrence of pyruvate involved in a six-membered ring ketal in the sponge polysaccharide. An initial suspicion regarding the occurrence of this substituent was the identification of an intense high-field $^{1}H$-signal at 1.48 ppm. The $^{13}C,^{1}H$ HMBC spectrum (Fig. 4*B*) showed a double signal at $\delta_H/\delta_C$ 1.63/25.3 ppm and $\delta_H/\delta_C$ 1.31/25.3 ppm due to decoupling during the acquisition of the pulse sequence. These signals are clearly distinguishable from those assigned to $CH_3$ from fucose residues ($\delta_H/\delta_C$ at 1.38/16.0 ppm and $\delta_H/\delta_C$ 1.06/16.0). Moreover, we assigned two other signals coupled to the $\delta$ 1.48 frequency. These peaks resonate at $\delta_C$ 101.2 ppm and $\delta_C$ 175.2 ppm and correspond, respectively, to the groups O-C-O and COOH of the pyruvate. The up-field proton chemical shift of this system (1.48 ppm) (supplemental Table S5) clearly revealed a typical pyruvate involved in a six-membered cyclic ketal including O-4 and O-6 of a non-reducing terminal, potentially $\alpha$-galactose instead of a five-membered cyclic ketal (47, 48).

Fig. 5 summarizes the preponderant structure proposed for DaSP. This structure is a highly branched polymer constituting of a central core of 3-linked $\alpha$-glucose that is partially sulfated at 2 and 4 positions. The branches are composed of $\alpha$-Gal1→3-$\alpha$-Fuc2($SO_4$)1→3-$\alpha$-Glc4($SO_4$)1→3-$\alpha$-Glc, which is linked to position 4 of a $\alpha$-glucose unit in the central backbone. We also identified pyruvate groups involved in cyclic ketals with the positions O-4 and O-6 of $\alpha$-galactoses located at the non-reducing end. DaSP and oligosaccharides derived from the g200 of *M. prolifera* (22) share the same monosaccharide

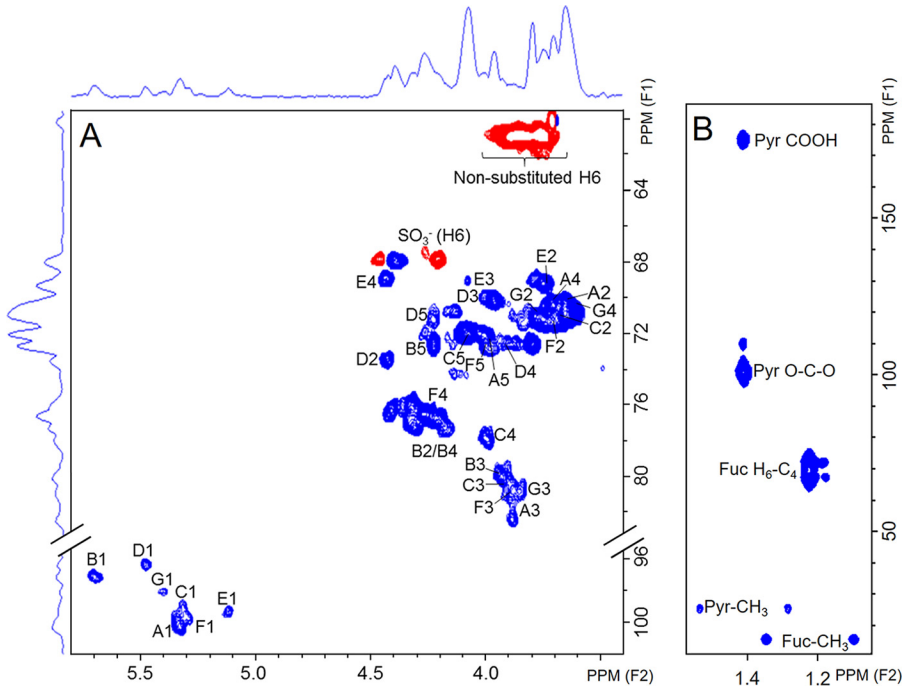


FIGURE 4. **Solution NMR analysis of DaSP.** *A*, $^{13}C,^{1}H$ HSQC spectrum; *blue peaks* are in-phase and belong to CH or $CH_3$ groups, whereas *red peaks* are anti-phase and belong to $CH_2$ groups. *B*, $^{13}C,^{1}H$ HMBC spectrum of the methyl region of the pyruvate groups and of fucose deoxy-C6. *Pyr-$CH_3$*, *Pyr O-C-O*, and *Pyr COOH* indicate signals from the $CH_3$, O-C-O, and COOH groups of the 4,6-*O*-(1′carboxyl)-ethylidene α-galactopyranosyl units, respectively.

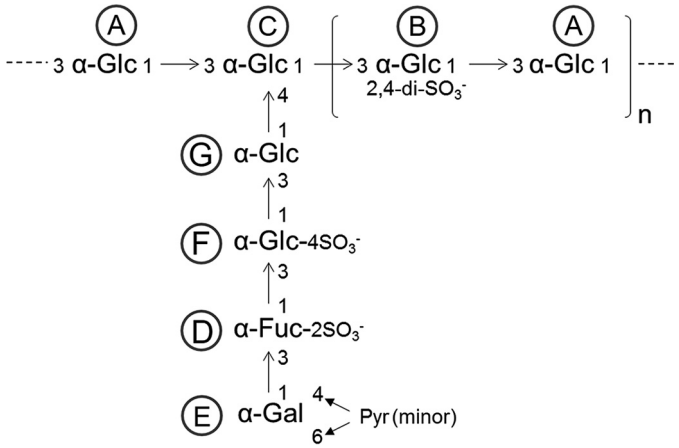


FIGURE 5. **Preponderant structure of DaSP.** *A*, α-Glc1→3. *B*, α-Glc(2,4-di-$SO_3^-$)1→3. *C*, α-Glc1→3. *D*, α-Fuc(2-$SO_3^-$)1→3. *E*, α-Gal(4,6-Pyr)1→3. *F*, α-Glc(4-$SO_3^-$)1→3. *G*, α-Glc1→4.

units except for the substitution of GlcNAc to glucose in DaSP; however, the sequence and proportion of these units in the polymers and their sulfation patterns greatly differ. Such differences are expected because the composition of sulfated polysaccharides from the AFs of sponges are allegedly species-specific (23).

*Self-interactions between DaSP Depend on Their Sulfate Groups and Exogenous Calcium*—To identify the reactive groups involved in the self-interaction of DaSP, we submitted the native molecule to a solvolysis reaction (to remove sulfate groups) or to a carboxyl reduction (to remove carboxyl groups present in the 4,6-*O*-pyruvate galactose residues). The efficiency of these chemical modifications was evidenced by the failure to detect sulfate content in derivatives submitted to solvolysis and sugar carboxyl groups in reduced derivatives (data not shown).

We initially investigated the self-interactions of native and modified DaSP using affinity chromatography in which native DaSP was coupled to Sepharose CL-4B. Native (Fig. 6*A*), carboxyl-reduced (Fig. 6*B*) and desulfated (Fig. 6*C*) DaSP were eluted with increasing concentrations of NaCl in solutions containing either 10 mM $CaCl_2$ (Fig. 6, *A*–C, *red triangles*) or 5 mM EDTA (Fig. 6, *A*–C, *black circles*). Native and carboxyl-reduced, but not desulfated DaSP, were retained in the column in the presence of calcium, indicating that sulfate groups are indispensable to promote chemical interactions between DaSP. These interactions are clearly calcium-dependent because they are completely abolished in the presence of EDTA.

We also assessed the capacity of native and modified DaSP to mediate the aggregation of amidine-latex beads coated with these polysaccharides. This model mimics the conspicuous aggregation process whereby dissociated sponge cells undergo when kept in culture (15). Beads coated with native and carboxyl-reduced DaSP and incubated in CMFTSW supplemented with 10 mM $CaCl_2$ (Fig. 6, *D* and *E*, respectively, and Fig. 6*J*), were able to effectively aggregate, unlike beads coated with the desulfated derivative (Fig. 6, *F* and *J*), indicating that sulfate but not carboxyl groups are necessary to promote aggregation. However, the aggregation was nearly abolished when beads were incubated in CMFTSW supplemented with 5 mM EDTA (Fig. 6, *G* and I, and Fig. 6*J*), further illustrating the calcium dependence of this aggregation process. The hexose content of hydrolyzed beads measured after the aggregation assays indicated an efficient polysaccharide coating (Fig. 6*K*), confirming that the absence of aggregation was not due to the absence of DaSP on the beads. The results presented above indicate the

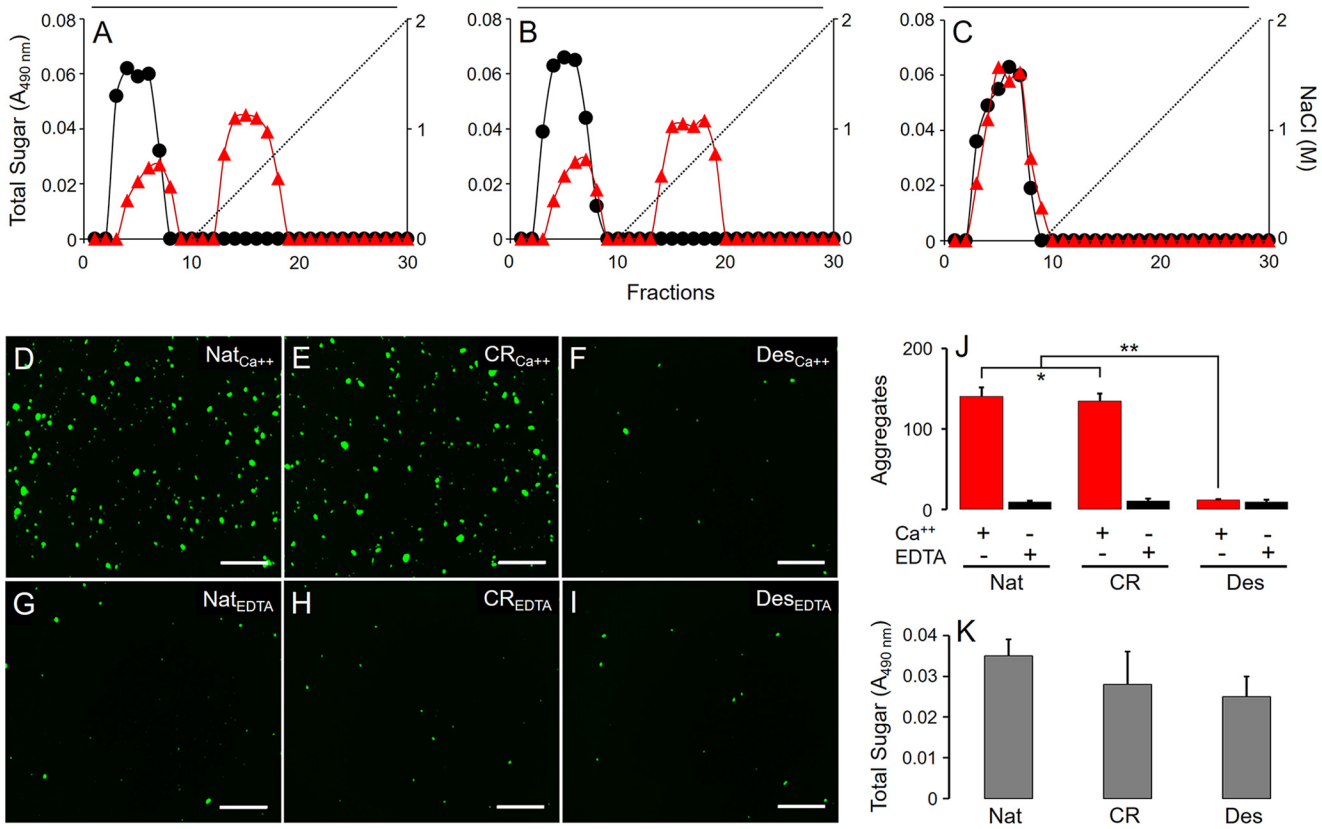


FIGURE 6. **Chemical interactions and aggregative capabilities of native and chemically modified DaSP.** Native (*A*), carboxyl-reduced (*B*), and desulfated (*C*) DaSPs were applied to a column containing Sepharose CL-4B coupled with native DaSP and eluted with NaCl solutions containing 5 mM EDTA (*black circles*) or 10 mM $CaCl_2$ (*red triangles*). Amidine-latex beads (1 $\mu$M) coated with native (*D* and *G*), carboxyl-reduced (*E* and *H*), and desulfated (*F* and *I*) DaSPs were incubated in CMFTW supplemented with 10 mM $CaCl_2$ (*D*, *E*, and *F*), or 5 mM EDTA (*G*, *H*, and *I*). *Scale bar* = 500 $\mu$m. *J*, number of aggregates (mean ± S.E.) formed by beads coated with native (*Nat*), carboxyl-reduced (*CR*), and desulfated (*Des*) DaSP in the presence ($Ca^{2+}$, *red*) or absence (*EDTA*, *black*) of calcium. *, $p > 0.05$; **, $p < 0.001$ (analysis of variance). *K*, total hexose content bound to the beads after the assays.

pivotal role played by the sulfate esters of DaSP in the homophilic and calcium-dependent self-interactions responsible for sponge cell adhesion.

*Sulfated DaSP Presents Stronger and Longer-lasting Self-interactions Than Its Desulfated Derivative*—After the dependence on sulfate groups to promote effective self-interactions between DaSPs was established, we characterized the physical features of these interactions using AFM-SMFS and -DFS techniques. These assays were performed using a well established method for the immobilization of biomolecules via a heterobifunctional PEG linker, which adds distance and steric flexibility for the binding partners and reduces unspecific interactions (49). Self-interactions of native and carboxyl-reduced DaSPs in the presence of CMFTSW supplemented with 10 mM $CaCl_2$ exhibited dissociation forces ($F_{max}$) between 151 and 212 pN (Fig. 7). The desulfated DaSP showed slightly weaker self-interaction forces between 99 and 176 pN that were similar to those obtained in the absence of calcium (CMFTSW supplemented with 5 mM EDTA), which ranged from 81 to 159 pN (Fig. 7). Despite slight differences, the forces between sulfated and desulfated DaSP and between assays carried out in the presence or absence of calcium had the same order of magnitude (Fig. 7). Thus, the absolute binding forces obtained in the SMFS assays should not be considered a dominant parameter in explaining the self-interactions of sulfated polysaccharides from AFs.

A deeper investigation on the self-interactions of native and chemically modified DaSP was accomplished using DFS assays in which the retraction velocity of the AFM cantilever was varied from 200 to 5000 nm $s^{-1}$ (Figs. 7 and 8*A*). According to the standard model of thermally driven dissociation under external force, the Bell-Evans model (36), an increase in the average dissociation force ($F_{max}$) is expected with larger loading rates (Fig. 8*B*) following Equation 1,

$$F_{max} = \frac{k_B T}{x_\beta} \ln \frac{x_\beta r}{k_B T k_{off}} \qquad \text{(Eq. 1)}$$

where $k_B T$ denotes the thermal energy, $r$ is the loading rate obtained by multiplying the retraction velocity by the molecular elasticity of the system, and $x_\beta$ is the reaction length representing the distance between the minimum of the binding potential and the transition state that separates bound from free states. In a DFS plot $F_{max}$ values are plotted against their respective loading rates in a semi-logarithmic manner (Fig. 8*B*). $k_{off}$ is the thermal off-rate constant under zero external load and can be deduced by linearly extrapolating the data in the DFS plot to zero external force ($F = 0$); the slope of the linear fit can be assigned to the inverse reaction length ($x_\beta^{-1}$). In addition to the reaction length, a second important parameter that can be derived from DFS data is the

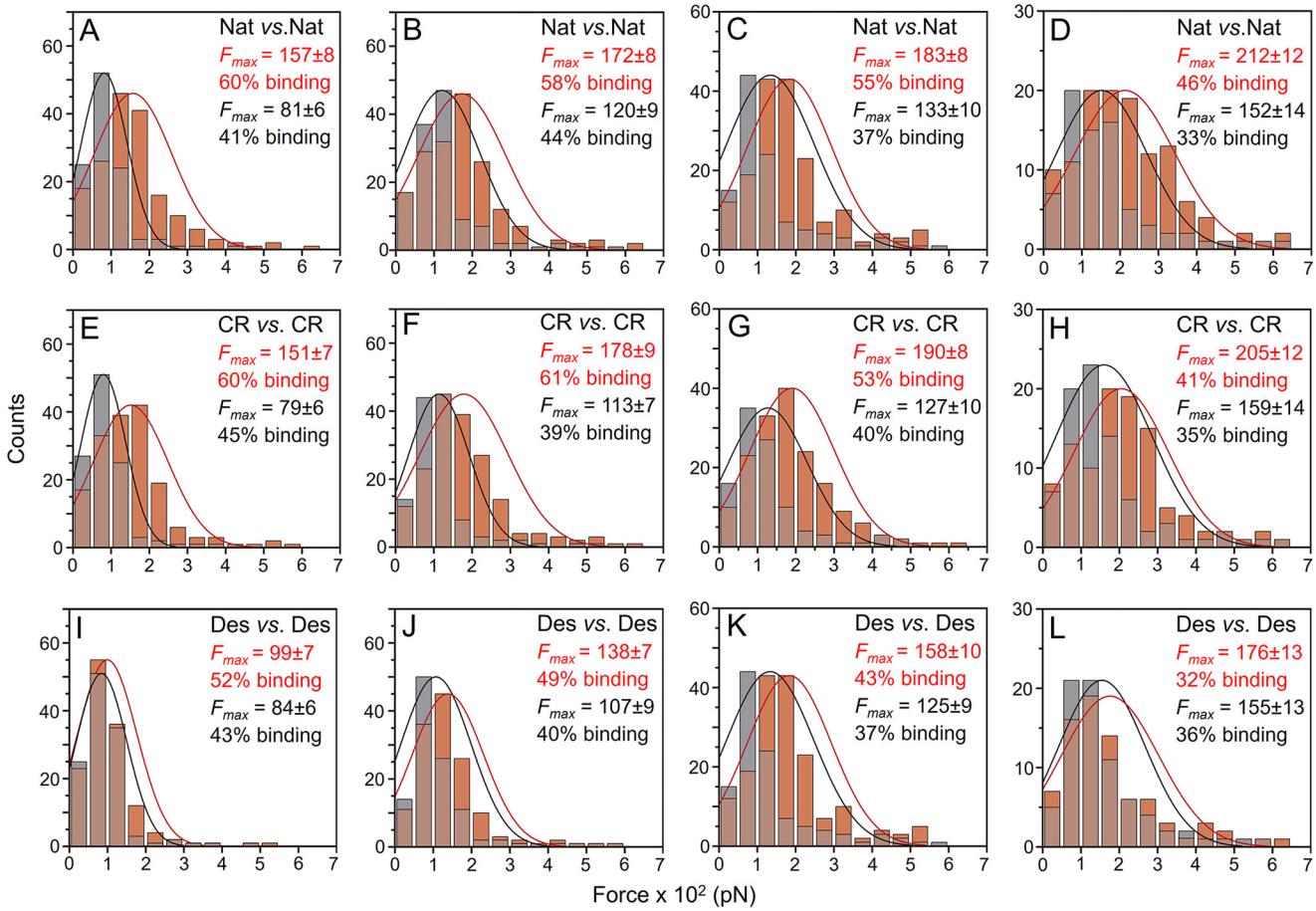


FIGURE 7. **AFM-SMFS analysis of native and chemically modified DaSP.** Force histograms of self-interactions of native (*A*, *B*, *C*, and *D*), carboxyl-reduced (*E*, *F*, *G*, and *H*), and desulfated (*I*, *J*, *K*, and *L*) DaSPs in the presence (10 mM $CaCl_2$; *light red bars* and *red lines*) and absence (5 mM EDTA; *gray bars* and *black lines*) of calcium obtained at different retraction velocities: 200 nm·$s^{-1}$ (*A*, *E*, and *I*), 800 nm·$s^{-1}$ (*B*, *F*, and *J*), 2000 nm·$s^{-1}$ (*C*, *G*, and *K*), and 5000 nm·$s^{-1}$ (*D*, *H* and *L*). *Nat*, native; *CR*, carboxyl-reduced; *Des*, desulfated DaSP. The *inset* values for $F_{max}$ refer to the mean ± S.E. pN.

mean lifetime of the complex ($\tau$), which is inversely related to the $k_{off}$ ($\tau = k_{off}^{-1}$).

The DFS plot of our data showed the expected linear dependence according to the Bell-Evans model (Fig. 8*B*). Assays conducted in the presence of calcium with native and carboxyl-reduced DaSP presented clear differences with the desulfated derivative as well as with the assays conducted in the absence of calcium. In the presence of calcium the reaction length $x_\beta$ of self-interactions between native and carboxyl-reduced DaSPs was similar (~3.5 Å), whereas between desulfated DaSP and for all samples in the absence of calcium the reaction lengths were significantly shorter, ranging from 2.1 to 2.4 Å (Fig. 8*C*, supplemental Table S6).

The self-interaction lifetime $\tau$ of native and carboxyl-reduced DaSPs in the presence of calcium was orders of magnitude higher than for assays conducted with desulfated DaSP or in the absence of calcium (Fig. 8*D*, supplemental Table S6). The lifetime of the binding complex dramatically affects its stability because a rapid on-off switching between bound and unbound states is more susceptible to dissociation than longer interactions (5). Therefore, our AFM-SMFS and -DFS results unequivocally show that the calcium-mediated self-interactions of sulfated DaSPs are stronger and last longer than desulfated DaSP despite slightly differing average forces.

## Discussion

We herein showed that the aggregation factor of the sponge *D. anchorata* (DAF) has a circular supramolecular structure and multiple intermolecular binding sites, which places this proteoglycan within the spongican family (15). The structure of DAF sulfated polysaccharide (DaSP), which was characterized using solution NMR analysis, consists of a central backbone composed of α-Glc units partially sulfated at 2- and 4-positions and branches of Pyr(4,6)α-Gal→α-Fuc2($SO_3$)→α-Glc4($SO_3$)→α-Glc→; this was the first time that the structure of a complex-sulfated polysaccharide from sponge was fully determined. We also demonstrated through a variety of cell-free techniques that the calcium- and sulfate-mediated self-interactions between sulfated polysaccharides of AFs are responsible for sustaining cell adhesion in sponges.

Carbohydrate-carbohydrate interactions have been increasingly associated with several cell surface events (9–12). The vast structural plasticity of carbohydrates confers many combinatorial possibilities for fine-tuning cell-cell recognition, and their weak and reversible multivalent self-interactions endow strength and flexibility during the formation and maintenance of multicellular tissues (9). Several biological processes such as the early steps of embryo formation,

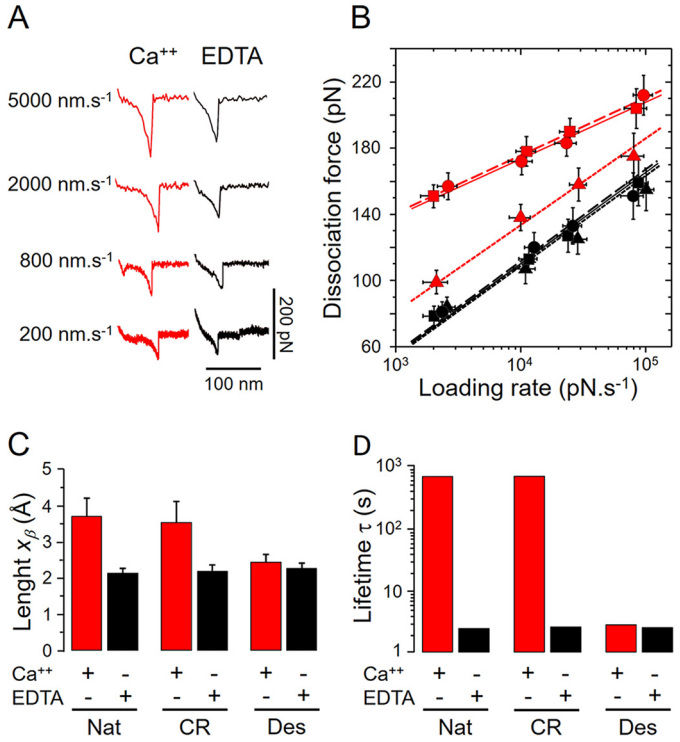


FIGURE 8. **DFS analysis of the self-interactions between native and chemically modified DaSP.** *A*, typical force curves of native DaSP obtained in the presence (*red*) or absence (*black*) of calcium with different retract velocities. *B*, DFS plot of native (*circles*, *solid lines*), carboxyl-reduced (*squares*, *dashed lines*), and desulfated (*triangles*, *dotted lines*) DaSP in the presence (*red*) or absence (*black*) of calcium showing the measured dissociation forces against the respective loading rates in a semi-logarithmic scale. *C*, reaction lengths $x_\beta$ (mean ± S.D.) of the self-interactions between native (*Nat*) and carboxyl-reduced (*CR*) and desulfated (*Des*) DaSP in the presence ($Ca^{2+}$, *red*) or absence (EDTA, *black*) of calcium. *D*, mean lifetime $\tau$ ($k_{off}^{-1}$) of the self-interactions between native (*Nat*) and carboxyl-reduced (*CR*) and desulfated (*Des*) DaSP in the presence ($Ca^{2+}$, *red*) or absence (*EDTA*, *black*) of calcium plotted in a logarithmic scale.

metastasis, and cell-cell adhesion events are mediated by carbohydrate-carbohydrate interactions by means of van der Waals contacts, hydrogen bonds, electrostatic forces, and bridges of divalent ions (9, 50).

As demonstrated here and elsewhere (*e.g.* Ref. 17), the homophilic and calcium-dependent self-interactions between sulfated polysaccharides components of AFs are the primary forces driving cell-cell adhesion in sponges. These interaction forces have been attributed to hydrogen bonds between the hydroxyl groups of sugar moieties of polysaccharides (10). In this model calcium ions are responsible only for the approach and organization of the sugar moieties and provide adequate surfaces for further interactions (5). However, the participation of the highly reactive sulfate groups of these polysaccharides was formerly speculated (20). More recently, this participation was deduced from SMFS measurements of stronger self-interaction forces in sulfated than in non-sulfated synthetic oligosaccharides derived from the AF of the sponge *M. prolifera* (27).

Our affinity chromatography data, bead aggregation assays, and measurements of single-molecule binding forces, lengths, and stabilities of native and chemically carboxyl-reduced and desulfated polysaccharides from AFs of the sponge *D. anchorata* clearly demonstrate the active participation of sulfate esters but not carboxyl groups in the calcium-dependent carbohydrate-carbohydrate interactions in sponges. Such sulfate dependence led us to hypothesize that the anionic sulfate groups of polysaccharides from adjacent AFs interact through calcium bridges with individual binding lengths of ~3.5 Å (Fig. 9). These calcium- and sulfate-mediated interactions provide the strength and stability (binding lifetime $>10^2$ s) necessary to sustain the aggregative properties of AFs and hence the physiological maintenance of cell-cell adhesion. Similar self-interactions mediated by calcium have been observed for the sulfated polysaccharide g200 from the AF of *M. prolifera* (5), indicating that such a mechanism of intermolecular interaction could be conspicuous in sponges.

We also observed significant binding forces between the desulfated derivative in either the presence or absence of calcium and between sulfated DaSPs in the absence of calcium. However, the binding forces of these interactions are weaker and markedly less stable (binding lifetime <10 s), and their reaction lengths fall below the hydrogen bond distance, which is ~2.9 Å (51). Similar characteristics were observed for the calcium-free self-interactions of g200 from *M. prolifera* (5). These calcium- and/or sulfate-free interactions likely operate through hydrogen bonds between hydroxyl groups on the polysaccharides, whereas the excess of $Na^+$ ions in seawater neutralizes the repulsive forces expected from the highly anionic sulfate and carboxyl groups (10). The ability of calcium ions to provide adequate molecular landscapes for such interactions (5) was also observed because the binding forces measured for the desulfated derivative in the presence of calcium were slightly stronger than in experiments conducted in the absence of calcium.

Complex multiple binding events have been reported in other interactions involving carbohydrates, such as the interaction between heparin and the protein platelet factor 4, which is mediated by both electrostatic and hydrophobic bonds (52). Other example are the three different stable binding conformations formed between ricin and anti-ricin aptamer (53). Self-interactions of DaSP likely operate through both hydrogen bonds and sulfate-calcium bridges; however, the calcium- and/or sulfate-free interactions mediated by hydrogen bonds are unable to effectively sustain cell adhesion in sponges, as demonstrated here in aggregation assays with desulfated derivatives and elsewhere, for more than one century, by dissociating sponge tissues in calcium-free seawater (54).

Interestingly, the average self-interaction forces of DAF ($F_{max}$ 273 ± 6 pN) were substantially higher than native DaSP ($F_{max}$ 183 ± 8 pN) in experiments conducted in the presence of calcium and with the same retract velocity (2000 nm·$s^{-1}$), as previously reported for self-interactions of MAF and g200 (14). Because DaSP effectively mediates both interactions, similar single molecule forces are expected. Probably those stronger forces relate to a neat organization of DaSP units along the globular proteins in the DAF ring (Fig. 9), which may optimize their reactive landscapes, thus enhancing both the electrostatic interactions mediated by sulfate and calcium groups and the hydrogen bonds. Therefore, the organization of sulfated polysaccharides along the protein core of AFs possibly increases their self-interaction capabilities and hence the stability of cell-cell adhesion.

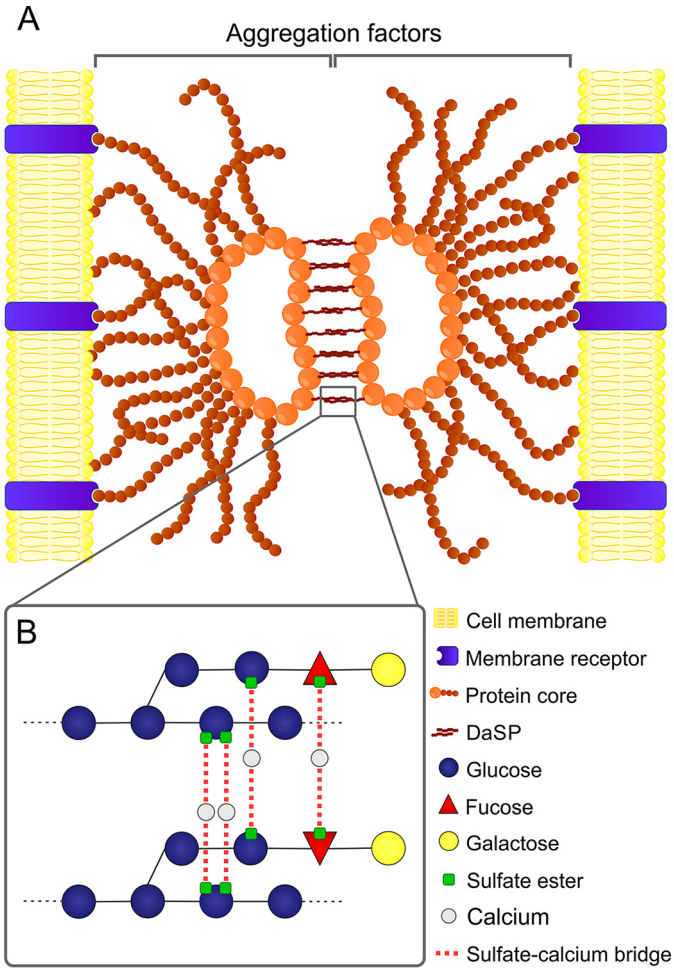


FIGURE 9. **Model representing the molecular mechanism of cell adhesion in sponges.** *A*, schematic view of the current model depicting the interaction of two aggregation factors attached to membrane receptors of two adjacent sponge cells, modified from (15). *B*, detail of the calcium- and sulfate-mediated self-interactions of the sulfated polysaccharide (DaSP) component of aggregation factors. The interactions, represented by *red dashed lines*, are schematic and do not represent the actual sulfate groups involved in each depicted interaction.

The first sponges likely began to diverge from single celled choanoflagellate-like ancestors at least 800 Ma, in the cryogenian period (2). The oldest sponge-like body fossils are found in shales dated between 660 and 635 Ma (mega-annum) and are thus before the oldest (579–565 Ma) Ediacaran macrofossil assemblages (55). Substantial evidence relates such sponge ancestry with the early development of an allorecognition system of sufficient complexity to enable individual self-nonself recognition (1), as indicated by the allelic polymorphism identified in MAF proteins and its correlation with tissue incompatibility reactions (56–58). The presence of this precise allorecognition may have had crucial evolutionary importance in ancestral sponges by preventing the negative effects of chimerism, such as the maintenance within the populations of fitness-reducing genes (5). Another pivotal evolutionary milestone provided by AFs involves their calcium-mediated interactions. The mean sponge cell disaggregation time is astonishingly high ($>10^{15}$ s, ~30 million years) in calcium-rich (10 mM) and reduced (<10 s) in calcium-deficient (0 mM) environments (5). Although this simulated number may not be meaningful on the level of an individual sponge, it dramatically illustrates that the calcium concentration in the extracellular environment can lead to either weakly aggregated cells or stable multicellular assemblies (5). The resulting strength and stability of the calcium-dependent cell adhesions mediated by AFs in ancestral sponges may have enabled them to maintain their integrity until reproduction, thereby permitting genetic constitutions to remain within a multicellular individual and be passed down in inheritance lineages (5). Our findings clearly demonstrate that the strength and stability of these calcium-mediated interactions intrinsically relate to the presence of sulfate epitopes on polysaccharides neatly organized along the AFs.

Sulfated polysaccharides are evolutionarily conserved and widely distributed among nearly all invertebrate phyla (59). Heparan sulfate-like glycosaminoglycans have been biochemically identified in phyla at the base of the metazoan lineage such as Cnidaria (60). Intriguingly, the choanoflagellate *Monosiga brevicollis* presents, although with low homologies, ortholog sequences to key heparan sulfate biosynthetic enzymes (61). Although heparan sulfate has not been thus far identified in sponges, the rudimentary biosynthetic machinery present in their putative single-celled ancestor possibly participated as a precursor of the enzymes involved in the synthesis of their own sulfated polysaccharides. Therefore, the early advent of sulfated polysaccharides biosynthesis may represent a crucial innovation involved in the development of ancestral sponges and hence triggered the evolution of the metazoan multicellular complexity.

Sponges are the oldest extant Precambrian metazoan phylum and thus are valid models to study the factors that could have led to the rise of multicellular animals. The Cambrian explosion was a relatively short period ~540 Ma that marked a general acceleration in the evolution of most animal phyla; however, the trigger of this key biological event remains elusive. We hypothesized that the Cambrian explosion may have been unleashed by the coincidence in time of primitive sponge-like metazoans endowed with 1) self/non-self-recognition, 2) adhesive sulfated polysaccharides, and 3) a surge in seawater calcium that increased the binding forces and stabilities between their calcium-dependent cell adhesion molecules (1, 5).

*Author Contributions*—E. V., J. J. V.-D, X. F.-B., and P. A. S. M. designed the research. E. V., G. R. C. S., R. S. A., and D. A. performed the research and analyzed the data. E. V., X. F.-B., and P. A. S. M. wrote the paper.

*Acknowledgments—We thank the Centro Nacional de Ressonância Magnética Nuclear Jiri Jonas for the access to the NMR spectrometers and Adriana Piquet and Mirian Funes for technical assistance.*

## References

1. Fernàndez-Busquets, X. (2010) Cambrian Explosion. *Encyclopedia of Life Sciences* (Kehrer-Sawatzki, H., ed) pp. 1–10, John Wiley & Sons, Chichester, UK
2. Peterson, K. J., and Butterfield, N. J. (2005) Origin of the Eumetazoa: testing ecological predictions of molecular clocks against the Proterozoic fossil record. *Proc. Natl. Acad. Sci. U.S.A.* **102,** 9547–9552
3. Philippe, H., Brinkmann, H., Lavrov, D. V., Littlewood, D. T., Manuel, M., Wörheide, G., and Baurain, D. (2011) Resolving difficult phylogenetic

questions: why more sequences are not enough. *PLoS Biol.* **9,** e1000602
4. Mills, D. B., Ward, L. M., Jones, C., Sweeten, B., Forth, M., Treusch, A. H., and Canfield, D. E. (2014) Oxygen requirements of the earliest animals. *Proc. Natl. Acad. Sci. U.S.A.* **111,** 4168–4172
5. Fernàndez-Busquets, X., Körnig, A., Bucior, I., Burger, M. M., and Anselmetti, D. (2009) Self-recognition and $Ca^{2+}$-dependent carbohydrate-carbohydrate cell adhesion provide clues to the Cambrian explosion. *Mol. Biol. Evol.* **26,** 2551–2561
6. Knoll, A. (2011) The multiple origins of complex multicellularity. *Annu. Rev. Earth Planet Sci.* **39,** 217–239
7. Abedin, M., and King, N. (2010) Diverse evolutionary paths to cell adhesion. *Trends Cell Biol.* **20,** 734–742
8. Jarchow, J., Fritz, J., Anselmetti, D., Calabro, A., Hascall, V. C., Gerosa, D., Burger, M. M., and Fernàndez-Busquets, X. (2000) Supramolecular structure of a new family of circular proteoglycans mediating cell adhesion in sponges. *J. Struct. Biol.* **132,** 95–105
9. Bucior, I., and Burger, M. M. (2004) Carbohydrate-carbohydrate interactions in cell recognition. *Curr. Opin. Struct. Biol.* **14,** 631–637
10. Spillmann, D., and Burger, M. M. (2000) Carbohydrate-carbohydrate interactions. *Carbohydrates in Chemistry and Biology: A Comprehensive Handbook* (Ernst, B., Hart, G. W., and Sinay, P., eds) pp. 1061–1091, Wiley-VCH, Weinheim, Germany
11. Eggens, I., Fenderson, B., Toyokuni, T., Dean, B., Stroud, M., and Hakomori S. (1989) Specific interaction between $Le^x$ and $Le^x$ determinants: a possible basis for cell recognition in preimplantation embryos and in embryonal carcinoma cells. *J. Biol. Chem.* **264,** 9476–9484
12. Kojima, N., and Hakomori, S. (1991) Cell adhesion, spreading, and motility of GM3-expressing cells based on glycolipid-glycolipid interaction. *J. Biol. Chem.* **266,** 17552–17558
13. Bucior, I., Scheuring, S., Engel, A., and Burger, M. M. (2004) Carbohydrate-carbohydrate interaction provides adhesion force and specificity for cellular recognition. *J. Cell Biol.* **165,** 529–537
14. Garcia-Manyes, S., Bucior, I., Ros, R., Anselmetti, D., Sanz, F., Burger, M. M., and Fernàndez-Busquets, X. (2006) Proteoglycan mechanics studied by single-molecule force spectroscopy of allotypic cell adhesion glycans. *J. Biol. Chem.* **281,** 5992–5999
15. Fernàndez-Busquets, X., and Burger, M. M. (2003) Circular proteoglycans from sponges: first members of the spongican family. *Cell. Mol. Life Sci.* **60,** 88–112
16. Blumbach, B., Pancer, Z., Diehl-Seifert, B., Steffen, R., Münkner, J., Müller, I., and Müller, W. E. (1998) The putative sponge aggregation receptor: isolation and characterization of a molecule composed of scavenger receptor cysteine-rich domains and short consensus repeats. *J. Cell Sci.* **111,** 2635–2644
17. Bucior, I., and Burger, M. M. (2004) Carbohydrate-carbohydrate interaction as a major force initiating cell-cell recognition. *Glycoconj. J.* **21,** 111–123
18. Misevic, G. N., Guerardel, Y., Sumanovski, L. T., Slomianny, M. C., Demarty, M., Ripoll, C., Karamanos, Y., Maes, E., Popescu, O., and Strecker, G. (2004) Molecular recognition between glyconectins as an adhesion self-assembly pathway to multicellularity. *J. Biol. Chem.* **279,** 15579–15590
19. Vilanova, E., Coutinho, C. C., and Mourão, P. A. (2009) Sulfated polysaccharides from marine sponges (Porifera): an ancestor cell-cell adhesion event based on the carbohydrate-carbohydrate interaction. *Glycobiology* **19,** 860–867
20. Popescu, O., Checiu, I., Gherghel, P., Simon, Z., and Misevic, G. N. (2003) Quantitative and qualitative approach of glycan-glycan interactions in marine sponges. *Biochimie* **85,** 181–188
21. Zierer, M. S., and Mourão, P. A. (2000) A wide diversity of sulfated polysaccharides are synthesized by different species of marine sponges. *Carbohydr. Res.* **328,** 209–216
22. Guerardel, Y., Czeszak, X., Sumanovski, L. T., Karamanos, Y., Popescu, O., Strecker, G., and Misevic, G. N. (2004) Molecular fingerprinting of carbohydrate structure phenotypes of three Porifera proteoglycan-like glyconectins. *J. Biol. Chem.* **279,** 15591–15603
23. Vilanova, E., Zilberberg, C., Kochem, M., Custódio, M. R., and Mourão P. A. S. (2007) A novel biochemical method to distinguish cryptic species of genus *Chondrilla* (Demospongiae: Chondrosida) based on its sulfated polysaccharides. In *Porifera Research: Biodiversity, Innovation, and Sustainability* (Custódio, M. R., *et al.*, eds) pp. 653–659, Museu Nacional, Rio de Janeiro, Brazil
24. Lindahl, U., and Höök, M. (1978) Glycosaminoglycans and their binding to biological macromolecules. *Annu. Rev. Biochem.* **47,** 385–417
25. Spillmann, D., and Burger, M. M. (1996) Carbohydrate-carbohydrate interactions in adhesion. *J. Cell Biochem.* **61,** 562–568
26. Haseley, S. R., Vermeer, H. J., Kamerling, J. P., and Vliegenthart, J. F. (2001) Carbohydrate self-recognition mediates marine sponge cellular adhesion. *Proc. Natl. Acad. Sci. U.S.A.* **98,** 9419–9424
27. Lorenz, B., Álvarez de Cienfuegos, L., Oelkers, M., Kriemen, E., Brand, C., Stephan, M., Sunnick, E., Yüksel, D., Kalsani, V., Kumar, K., Werz, D. B., and Janshoff, A. (2012) Model system for cell adhesion mediated by weak carbohydrate-carbohydrate interactions. *J. Am. Chem. Soc.* **134,** 3326–3329
28. Vilanova, E., Coutinho, C., Maia, G., and Mourão, P. A. (2010) Sulfated polysaccharides from marine sponges: conspicuous distribution among different cell types and involvement on formation of *in vitro* cell aggregates. *Cell Tissue Res.* **340,** 523–531
29. Aquino, R. S., Pereira, M. S., Vairo, B. C., Cinelli, L. P., Santos, G. R., Fonseca, R. J., and Mourão, P. A. (2010) Heparins from porcine and bovine intestinal mucosa: are they similar drugs? *Thromb. Haemost.* **103,** 1005–1015
30. Bax, A., and Davis, D. G. (1985) Practical aspects of two-dimensional transverse NOE spectroscopy. *J. Magn. Reson.* **63,** 207–213
31. Santos, G. R., Glauser, B. F., Parreiras, L. A., Vilanova, E., and Mourão, P. A. (2015) Differences in $\alpha$-fucose branch structures of sea cucumber fucosylated chondroitin sulfates do not affect their anticoagulant activity. *Glycobiology* **25,** 1043–1052
32. Nagasawa, K., Inoue, Y., and Kamata, T. (1977) Solvolytic desulfation of glycosaminoglycuronan sulfates with dimethyl sulfoxide containing water or methanol. *Carbohydr. Res.* **58,** 47–55
33. Taylor, R. L., Shively, J. E., and Conrad, H. E. (1976) Stoichiometric reduction of uronic acid carboxyl groups in polysaccharides. in *Methods in Carbohydrate Chemistry*, Vol. 7 (Whistler, R. L., Wolfrom, M. L., and BeMiller, J. N., eds), pp. 149–151, Academic Press, New York
34. Hegner, M., Wagner, P., and Semenza, G. (1993) Ultralarge atomically flat template-stripped Au surfaces for scanning probe microscopy. *Surf. Sci.* **291,** 39–46
35. Lévy, R., and Maaloum, M. (2002) Measuring the spring constant of atomic force microscope cantilevers: thermal fluctuations and other methods. *Nanotechnology* **13,** 33–37
36. Merkel, R., Nassoy, P., Leung, A., Ritchie, K., and Evans, E. (1999) Energy landscapes of receptor-ligand bonds explored with dynamic force spectroscopy. *Nature* **397,** 50–53
37. Dammer, U., Popescu, O., Wagner, P., Anselmetti, D., Güntherodt, H. J., and Misevic, G. (1995) Binding strength between cell adhesion proteoglycans measured by atomic force microscopy. *Science* **267,** 1173–1175
38. Morrow, C., and Cárdenas, P. (2015) Proposal for a revised classification of the Demospongiae (Porifera). *Front. Zool.* **12,** 7
39. Alves, A. P., Mulloy, B., Diniz, J. A., and Mourão, P. A. (1997) Sulfated polysaccharides from the egg jelly layer are species-specific inducers of acrosomal reaction in sperms of sea urchins. *J. Biol. Chem.* **272,** 6965–6971
40. Vilela-Silva, A. C., Castro, M. O., Valente, A. P., Biermann, C. H., and Mourao, P. A. (2002) Sulfated fucans from the egg jellies of the closely related sea urchins *Strongylocentrotus droebachiensis* and *Strongylocentrotus pallidus* ensure species-specific fertilization. *J. Biol. Chem.* **277,** 379–387
41. Lundborg, M., and Widmalm, G. (2011) Structural analysis of glycans by NMR chemical shift prediction. *Anal. Chem.* **83,** 1514–1517
42. Huang, Q., and Zhang, L. (2005) Solution properties of (1→3)-$\alpha$-D-glucan and its sulfated derivatives from *Poria cocos* mycelia via fermentation tank. *Biopolymers* **79,** 28–38
43. Bao, X., Duan, J., Fang, X., and Fang, J. (2001) Chemical modifications of the (1→3)-$\alpha$-D-glucan from spores of *Ganoderma lucidum* and investigation of their physicochemical properties and immunological activity. *Car-*

*bohydr. Res.* **336,** 127–140
44. Pereira, M. S., Vilela-Silva, A. C., Valente, A. P., and Mourão, P. A. (2002) A 2-sulfated, 3-linked α-L-galactan is an anticoagulante polysaccharide. *Carbohydr. Res.* **337,** 2231–2238
45. Alves, A. P., Mulloy, B., Moy, G. W., Vacquier, V. D., and Mourão, P. A. (1998) Females of the sea urchin *Strongylocentrotus purpuratus* differ in the structures of their egg jelly sulfated fucans. *Glycobiology* **8,** 939–946
46. Pavão, M. S., Mourão, P. A., and Mulloy, B. (1990) Structure of a unique sulfated α-L-galactofucan from the tunicate *Clavelina*. *Carbohydr. Res.* **208,** 153–161
47. Bilan, M. I., Vinogradova, E. V., Shashkov, A. S., and Usov, A. I. (2007) Structure of a highly pyruvylated galactan sulfate from the Pacific green alga *Codium yezoense* (Bryopsidales, Chlorophyta). *Carbohydr. Res.* **342,** 586–596
48. Farias, E. H., Pomin, V. H., Valente, A. P., Nader, H. B., Rocha, H. A., and Mourão, P. A. (2008) A preponderantly 4-sulfated, 3-linked galactan from the green alga *Codium isthmocladum*. *Glycobiology* **18,** 250–259
49. Hinterdorfer, P., Baumgartner, W., Gruber, H. J., Schilcher, K., and Schindler, H. (1996) Detection and localization of individual antibody-antigen recognition events by atomic force microscopy. *Proc. Natl. Acad. Sci. U.S.A.* **93,** 3477–3481
50. Koshy, K. M., and Boggs, J. M. (1996) Investigation of the calcium-mediated association between the carbohydrate head groups of galactosylceramide and galactosylceramide I3 sulfate by electrospray ionization mass spectrometry. *J. Biol. Chem.* **271,** 3496–3499
51. Mathews, C. K., and van Holde, K. E. (1990) *Biochemistry*, Benjamin/Cummings Publishing Co., San Francisco, CA
52. Nguyen, T. H., Greinacher, A., and Delcea, M. (2015) Quantitative description of thermodynamic and kinetic properties of the platelet factor 4/heparin bonds. *Nanoscale* **7,** 10130–10139
53. Wang, B., Park, B., Kwon, Y., and Xu, B. (2014) Determining the elastic properties of aptamer-ricin single molecule multiple pathway interactions. *Appl. Phys. Lett.* **104,** 193702
54. Wilson, H. V. (1907) On some phenomena of coalescence and regeneration in sponges. *J. Exp. Zool.* **5,** 245–258
55. Maloof, A. C., Rose, C., Beach, R., Samuels, B. M., Calmet, C. C., Erwin, D. H., Poirier, G. H., Yao, M., and Simons, R. J. (2010) Possible animal-body fossils in pre-Marinoan limestones from South Australia. *Nat. Geosci.* **3,** 653–659
56. Fernàndez-Busquets, X., and Burger, M. M. (1997) The main protein of the aggregation factor responsible for species-specific cell adhesion in the marine sponge *Microciona prolifera* is highly polymorphic. *J. Biol. Chem.* **272,** 27839–27847
57. Fernàndez-Busquets, X., Gerosa, D., Hess, D., and Burger, M. M. (1998) Accumulation in marine sponge grafts of the mRNA encoding the main proteins of the cell adhesion system. *J. Biol. Chem.* **273,** 29545–29553
58. Sabella, C., Faszewski, E., Himic, L., Colpitts, K. M., Kaltenbach, J., Burger, M. M., and Fernàndez-Busquets, X. (2007) Cyclosporin a suspends transplantation reactions in the marine sponge *Microciona prolifera*. *J. Immunol.* **179,** 5927–5935
59. Medeiros, G. F., Mendes, A., Castro, R. A., Baú, E. C., Nader, H. B., and Dietrich, C. P. (2000) Distribution of sulfated glycosaminoglycans in the animal kingdom: widespread occurrence of heparin-like compounds in invertebrates. *Biochim. Biophys. Acta* **1475,** 287–294
60. Yamada, S., Morimoto, H., Fujisawa, T., and Sugahara, K. (2007) Glycosaminoglycans in *Hydra magnipapillata* (Hydrozoa, Cnidaria): demonstration of chondroitin in the developing nematocyst, the sting organelle, and structural characterization of glycosaminoglycans. *Glycobiology* **17,** 886–894
61. Ori, A., Wilkinson, M. C., and Fernig, D. G. (2011) A systems biology approach for the investigation of the heparin/heparan sulfate interactome. *J. Biol. Chem.* **286,** 19892–19904